

# Crystal structure of the 500-kDa yeast acetyl-CoA carboxylase holoenzyme dimer

Jia Wei<sup>1</sup> & Liang Tong<sup>1</sup>

**Acetyl-CoA carboxylase (ACC) has crucial roles in fatty acid metabolism and is an attractive target for drug discovery against diabetes, cancer and other diseases<sup>1–6</sup>. *Saccharomyces cerevisiae* ACC (ScACC) is crucial for the production of very-long-chain fatty acids and the maintenance of the nuclear envelope<sup>7,8</sup>. ACC contains biotin carboxylase (BC) and carboxyltransferase (CT) activities, and its biotin is linked covalently to the biotin carboxyl carrier protein (BCCP). Most eukaryotic ACCs are 250-kilodalton (kDa), multi-domain enzymes and function as homodimers and higher oligomers. They contain a unique, 80-kDa central region that shares no homology with other proteins. Although the structures of the BC, CT and BCCP domains and other biotin-dependent carboxylase holoenzymes are known<sup>1,9–14</sup>, there is currently no structural information on the ACC holoenzyme. Here we report the crystal structure of the full-length, 500-kDa holoenzyme dimer of ScACC. The structure is remarkably different from that of the other biotin-dependent carboxylases. The central region contains five domains and is important for positioning the BC and CT domains for catalysis. The structure unexpectedly reveals a dimer of the BC domain and extensive conformational differences compared to the structure of the BC domain alone, which is a monomer. These structural changes reveal why the BC domain alone is catalytically inactive and define the molecular mechanism for the inhibition of eukaryotic ACC by the natural product soraphen A<sup>15,16</sup> and by phosphorylation of a Ser residue just before the BC domain core in mammalian ACC. The BC and CT active sites are separated by 80 Å, and the entire BCCP domain must translocate during catalysis.**

The primary sequences of the single-chain, multi-domain eukaryotic ACCs can be divided into three regions of roughly equal sizes. The amino-terminal region (residues 1–795 in ScACC, Fig. 1a) contains the BC and BCCP domains, with possibly a BT (BC–CT interaction) domain between them, as observed in the structures of propionyl-CoA carboxylase (PCC)<sup>11</sup> and 3-methylcrotonyl-CoA carboxylase (MCC)<sup>12</sup>. The carboxy-terminal region (residues 1492–2233) contains the N and C domains of CT<sup>17</sup>. The structure and function of the central region (residues 796–1491) are currently not known. It is not as well conserved among the eukaryotic ACCs (Extended Data Figs 1–3). BC catalyses the MgATP-dependent carboxylation of the N1' atom of biotin (Extended Data Fig. 4). The carboxybiotin (and BCCP) then translocates to the CT active site, where the substrate acetyl-CoA is carboxylated.

We expressed in *Escherichia coli* the 250-kDa ScACC (residues 22–2233) and determined its crystal structure at 3.2 Å resolution (Extended Data Table 1, Extended Data Fig. 4). The structure of the ScACC holoenzyme is remarkably different from that of the other biotin-dependent carboxylases<sup>9–14</sup>. The 500-kDa holoenzyme dimer obeys two-fold symmetry, and its overall structure is shaped like a quarter of a disk (Fig. 1b), with a radius of ~140 Å and thickness of ~120 Å (Fig. 1c), although there is a large channel measuring ~30 Å across through the centre of the holoenzyme (Extended Data Fig. 5). A BC domain dimer (Fig. 1d) is located near the centre of the

disk, while the CT domain dimer (Fig. 1e) forms a part of the edge of the disk. A BCCP domain is positioned near the centre of each face of the holoenzyme, and its biotin is located in the CT active site (Fig. 1b).

We have also determined the structure at 3.1 Å resolution of the holoenzyme where the BCCP domain is not biotinylated (Extended Data Table 1). The overall structure of this dimer is essentially the same as the other structure, with r.m.s. distance of 0.45 Å for their 3,928 equivalent C $\alpha$  atoms, although the BCCP domain is disordered in the absence of biotinylation. Earlier studies showed that biotinylation stabilizes *E. coli* BCCP<sup>18,19</sup>. This structure of the holoenzyme will not be discussed further here.

The overall structures of the two protomers of the holoenzyme are similar, with r.m.s. distance of 1.1 Å for 1,862 equivalent C $\alpha$  atoms located within 3 Å of each other after superposition. On the other hand, the r.m.s. distance is only 0.76 Å if the CT domains are superposed, and differences in the orientation and position of the other domains are visible, especially for the BC domain, which is located furthest from CT (Extended Data Fig. 4). Within CT, conformational differences in the small inserted domain<sup>17</sup> are observed (Extended Data Fig. 5), likely to be linked to differences in the position of BCCP in the two protomers, as the insert domain has direct contacts with BCCP.

The structure reveals that the central region of ScACC contains five domains, which we have named ACC central (AC) domains AC1 through AC5, giving a total of 10 major domains for each ScACC protomer (Fig. 1a). Domains AC1, AC2 and AC3 are all helical (Fig. 1f, Extended Data Fig. 2). AC1 contains three pairs of anti-parallel helices as well as inserts of a four-helical bundle (domain AC2, helices  $\alpha$ 3– $\alpha$ 6) and a helical hairpin ( $\alpha$ 8– $\alpha$ 9, Extended Data Fig. 5). AC3 is also a four-helical bundle but it has no interactions with AC1 and AC2, and instead is positioned between AC4 and AC5, mediating interactions between them. Domain AC4 is located at the end of the disk edge, and is separated from the AC4 domain of the other protomer by ~200 Å (Fig. 1b). Unexpectedly, the structure shows that AC4 and AC5 have similar backbone folds, consisting of a twisted  $\beta$ -sheet flanked on one face by helices (Extended Data Figs 4, 6). The r.m.s. distance is 2.9 Å for their equivalent C $\alpha$  atoms, but the sequence identity is only 12%. This backbone fold has weak similarity to a part of formamidase<sup>20</sup> (Extended Data Fig. 6) and several other enzymes, but the Z score is below 6.5 and the sequence identity is less than 9%<sup>21</sup>. The active sites of these enzymes are not conserved in AC4 or AC5. Therefore, this structural similarity is unlikely to have any functional significance for ACC.

The structure confirms the presence of a BT domain in the N-terminal region of ScACC (Fig. 1a). Its structure is similar to that in PCC<sup>11</sup>, with a central, long helix (Extended Data Fig. 4) surrounded by an eight-stranded anti-parallel  $\beta$ -barrel (Extended Data Fig. 5). The domain helps to mediate interactions between the BC and CT domains, as there are no direct contacts between them in the holoenzyme (Fig. 1b). Within each protomer, the last three strands of the BT domain  $\beta$ -barrel ( $\beta$ 27– $\beta$ 29) faces the BC domain (Figs 1b, 2a), while the C-terminal end of the long helix and the following loop connecting

<sup>1</sup>Department of Biological Sciences, Columbia University, New York, New York 10027, USA.

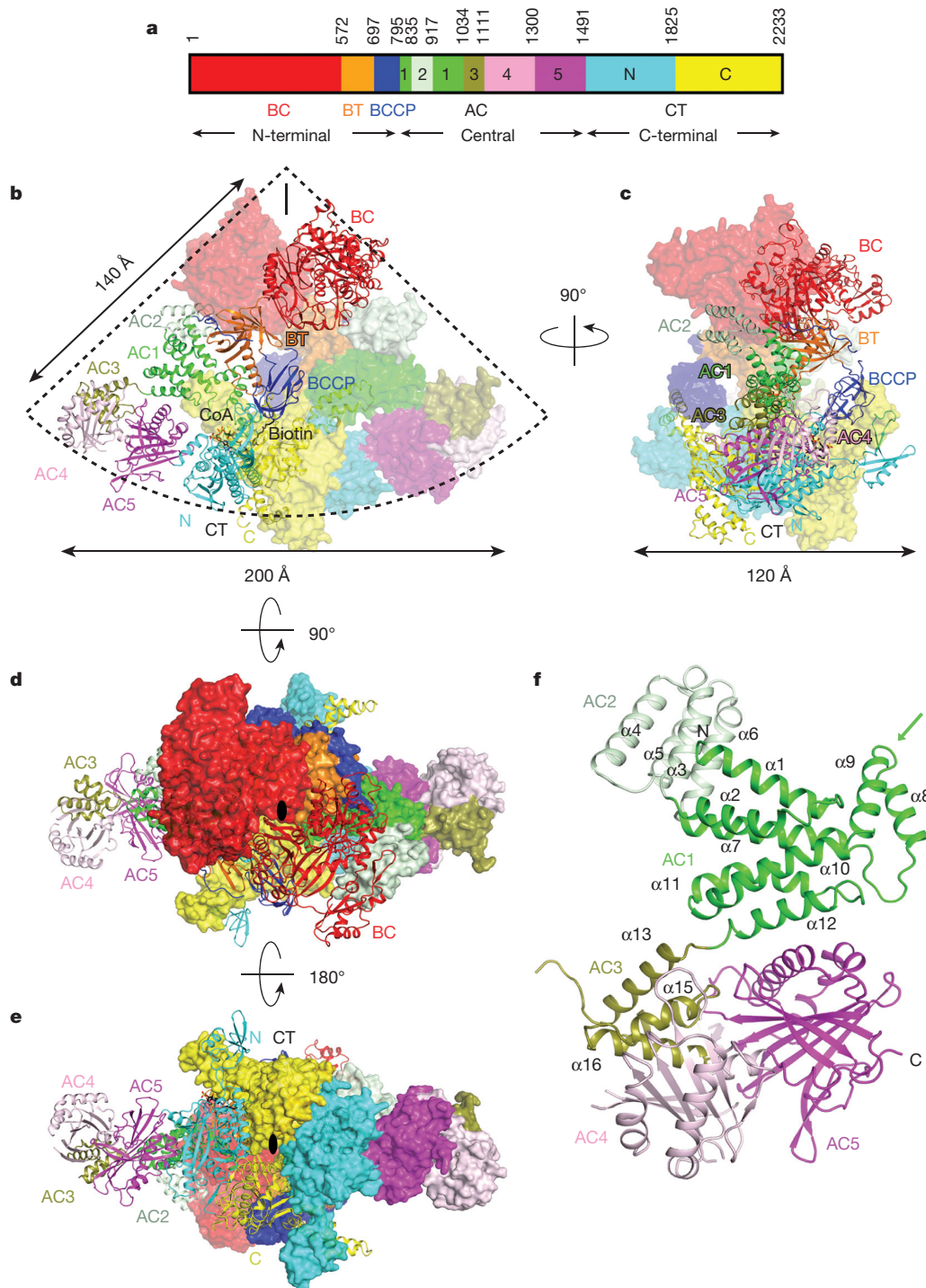
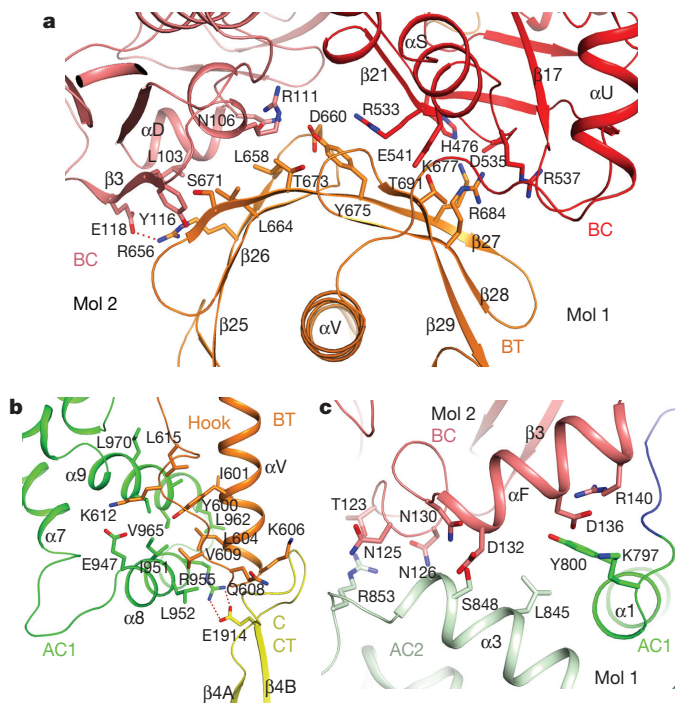


**Figure 1 | Crystal structure of the 500-kDa yeast acetyl-CoA carboxylase (ScACC) holoenzyme dimer.** **a**, Domain organization of ScACC. The three regions of the sequence are also indicated. AC, ACC central. **b**, Overall structure of ScACC holoenzyme dimer. One protomer is shown as ribbons while the other is shown only as a surface for clarity, both coloured according to **a**. The two-fold axis of the dimer is vertical (black line). **c–e**, Overall structure of

ScACC holoenzyme, viewed from the side (**c**), down the BC domain dimer (**d**), and down the CT domain dimer (**e**). The two-fold axis is indicated with the black oval. **f**, Structure of the five domains (AC1–AC5) in the central region of ScACC. The arrow points to the helical hairpin insert of AC1. The structure figures were produced with PyMOL (<http://www.pymol.org>).

to the first strand (the hook<sup>11</sup>) is flanked by the helical hairpin insert of AC1 ( $\alpha_8$ – $\alpha_9$ ) on one side and an inserted segment of a long loop between two  $\beta$ -strands ( $\beta$ 4A and  $\beta$ 4B) in the C domain of CT on the other side (Fig. 2b, Extended Data Fig. 4). In addition, a part of the long linker between the BCCP and AC1 domains has hydrophobic interactions with the top of one side of the BT domain  $\beta$ -barrel (Fig. 1b, Extended Data Fig. 5).

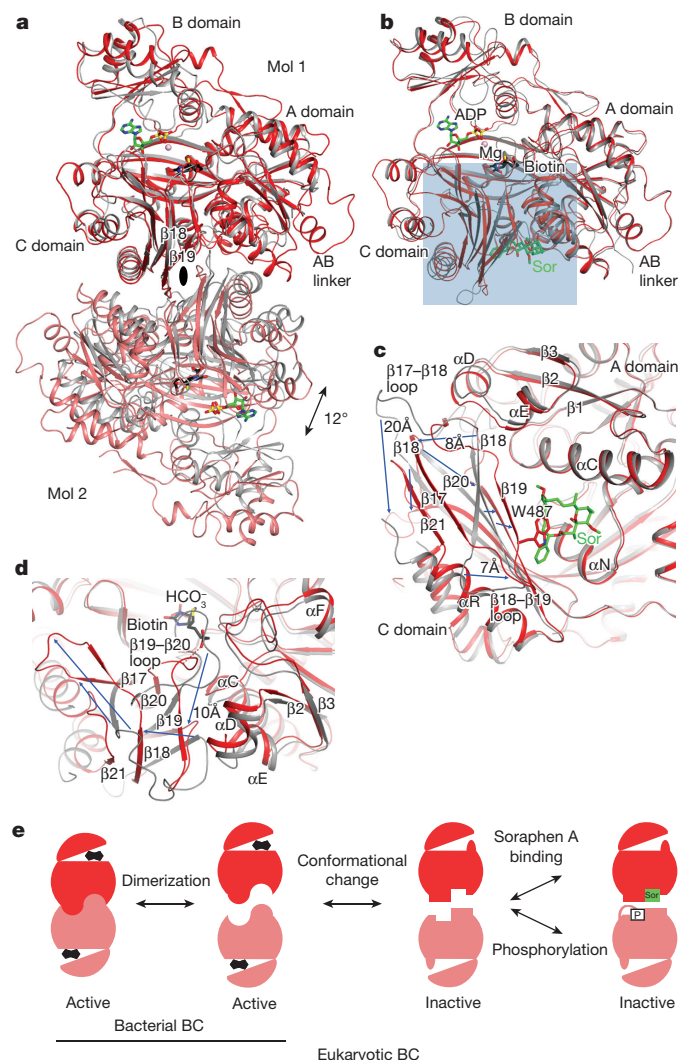
A total of  $\sim$ 9,000  $\text{\AA}^2$  of the surface area of each protomer is buried in the dimer interface, predominantly from the BC (1,200  $\text{\AA}^2$ , Extended Data Fig. 7) and CT (5,800  $\text{\AA}^2$ , Extended Data Fig. 8) domain dimers. The BC domain contributes an additional 900  $\text{\AA}^2$  through contacts with the BT domain (500  $\text{\AA}^2$ , Fig. 2a), AC1 (80  $\text{\AA}^2$ ) and AC2 (230  $\text{\AA}^2$ , Fig. 2c) of the other protomer. The BCCP domain buries  $\sim$ 400  $\text{\AA}^2$  in the CT active site, where it contacts the C domain of the



other protomer, but it is expected to translocate to the BC active site during catalysis (see later).

A major surprise from the structure is the observation of a BC domain dimer (Fig. 1d), because the BC domain alone is consistently a monomer and catalytically inactive based on earlier studies<sup>15,16,22,23</sup>. Moreover, the organization of this BC domain dimer is similar to that of the BC subunit dimer of *E. coli* ACC<sup>24–26</sup> (Fig. 3a), with a mostly hydrophilic interface (Extended Data Fig. 7). However, the structure of BC domain alone is incompatible with such a dimer due to steric clashes between the two molecules<sup>16</sup> (Extended Data Fig. 7). Large conformational changes for residues in the dimer interface are therefore necessary for the formation of this dimer, primarily involving the  $\beta$ -strands and connecting loops in the C sub-domain of BC (Fig. 3b). Especially, strand  $\beta 18$  moves by  $\sim 8 \text{ \AA}$ , taking it out of the central  $\beta$ -sheet of the C-domain (Fig. 3c, Supplementary Video 1).  $\beta 18$  instead forms a  $\beta$ -sheet with a new strand,  $\beta 21$ , which is not present in the structure of BC domain alone. Residues in the  $\beta 17$ - $\beta 18$  loop move by up to  $20 \text{ \AA}$ , and those in the  $\beta 18$ - $\beta 19$  loop by up to  $7 \text{ \AA}$  (Fig. 3c). In addition, the main chain of neighbouring strands  $\beta 17$ ,  $\beta 19$  and  $\beta 20$  shifts by  $\sim 3 \text{ \AA}$ . The new  $\beta 18$ -loop- $\beta 19$  structure is in the centre of the BC domain dimer (Fig. 3a), where the tip of this loop contacts the side chain of Trp487 in the other protomer (Extended Data Fig. 7).

The two distinct conformations of this domain explain why it is catalytically inactive on its own<sup>15</sup> and also define the molecular mechanism for the inhibition of eukaryotic ACC by the natural product soraphen A<sup>16</sup> and by phosphorylation of a Ser residue just before the BC domain core in mammalian ACC (Ser80 in human ACC1 and Ser222 in ACC2)<sup>23</sup> (Extended Data Fig. 1). As a part of the conformational change, residues in the  $\beta 19$ - $\beta 20$  loop move by up to  $10 \text{ \AA}$  (Fig. 3d, Supplementary Video 2). This loop in the structure of BC domain alone is likely to interfere with the binding of BCCP-biotin (Fig. 3d, Extended Data Fig. 7), based on the



binding mode of biotin to *E. coli* BC<sup>26</sup>. Consequently, BC domain alone is catalytically inactive because it assumes a conformation that cannot bind the BCCP-biotin substrate.

Soraphen A recognizes the conformation of isolated BC domain<sup>16</sup>, and this binding site does not exist in the BC domain dimer in the holoenzyme owing to the structural changes (Fig. 3c). For example, strands  $\beta 19$  and  $\beta 20$  move into the binding site, and especially the side

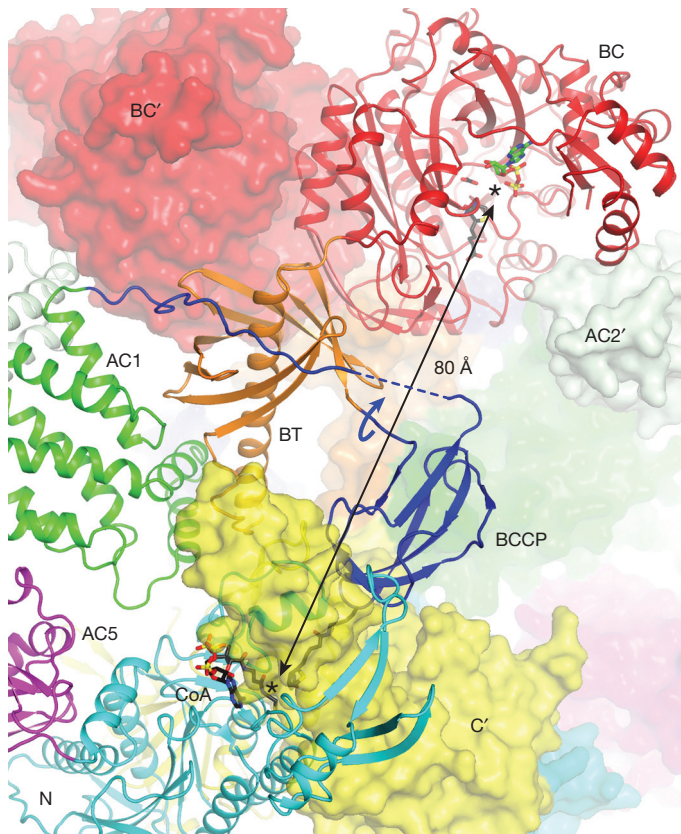


**Figure 4 | Translocation of BCCP and biotin during ACC catalysis.** The BC and CT active sites (black asterisks) of ScACC are separated by  $\sim 80 \text{ \AA}$  (arrow). A rotation of  $\sim 180^\circ$  around the BT-BCCP linker (curved arrow in blue) could place the biotin into the BC active site. The prime in the labels indicates the second protomer. The binding modes of ADP (green) and biotin (black) to *E. coli* BC subunit are shown as stick models<sup>26</sup>.

chain of Trp487 ( $\beta 19$ ) is in direct clash with soraphen A (Fig. 3c, Extended Data Fig. 7). Therefore, soraphen A inhibits the enzyme allosterically by stabilizing a catalytically inactive conformation of the BC domain. In the context of the holoenzyme, soraphen A binding will disrupt the formation of BC domain dimer (Fig. 1d), as the other protomer clashes with the compound as well (Extended Data Fig. 7). This could also be detrimental for catalysis as the BC domains may not be positioned correctly to accept the BCCP-biotin for carboxylation.

Upon phosphorylation, the peptide segment containing pSer222 of human ACC2 is located in the same binding site as soraphen A<sup>23</sup>, and the Trp487 side chain in the holoenzyme structure also clashes with this segment (Extended Data Fig. 7). Therefore, phosphorylation of this Ser residue inhibits the enzyme through the same mechanism as that of soraphen A. These structural observations greatly extend a model for the inhibitory mechanism proposed earlier<sup>25</sup> (Fig. 3e). ScACC does not have an equivalent phosphorylation site in this region of the sequence.

In comparison, the structure of the CT domain dimer in the holoenzyme is essentially the same as that of the domain alone<sup>17</sup>, with r.m.s. distance of  $0.61 \text{ \AA}$  among their equivalent  $C\alpha$  atoms (Extended Data Fig. 8). The binding of both BCCP-biotin and CoA (Extended Data Fig. 4) in one of the CT active sites provides direct insights into the catalysis by this enzyme. The thiol group of CoA is  $4.3 \text{ \AA}$  away from the N1' atom of biotin (Extended Data Fig. 8). Therefore, the two substrates are likely to be in the correct positions for catalysis. The position of biotin clashes with that of the compound CP-640186 (Extended Data Fig. 8), a nanomolar inhibitor of mammalian ACCs<sup>27</sup>, confirming that it functions by blocking biotin binding to the CT active site<sup>28</sup>.

Prior to the structure determination of the holoenzyme, we obtained the crystal structures for residues 797–1033 (domains AC1–AC2), 1036–1503 (AC3–AC5), and 569–1494 (BT, BCCP and the entire central region) (Extended Data Table 1). Comparisons of the structures of these domains alone with that of the holoenzyme reveal substantial variability in the relative positioning of the domains. Domains AC3–AC4 in the structure of AC3–AC5 alone can be readily superposed with those in the holoenzyme, but then the orientation of domain AC5 differ by  $40^\circ$  (Extended Data Fig. 9). Even more variability is observed in the structure of BT–BCCP–AC1–AC5 alone, illustrated by the differences in the positioning of AC1–AC2 relative to the BT domain and AC3–AC5 (Extended Data Fig. 9). Interestingly, between the two unique copies of the BT–BCCP–AC1–AC5 molecule in the crystal, one has a conformation of AC3–AC5 that is very similar to that in the holoenzyme (Extended Data Fig. 9), while the other is similar to that in AC3–AC5 alone, suggesting that domains AC3–AC5 may assume two (or more) distinct conformations.

Another discovery from the structure is that the central region has minimal contributions to the formation of the dimer. Besides the  $\sim 300 \text{ \AA}^2$  surface area burial for AC1 and AC2 (Fig. 2c), the central region has no contacts with the other protomer (Fig. 1b). On the other hand, the structure suggests that the central region is important for maintaining the BC and CT dimers in the correct relative positions for catalysis. The CT domain dimer is sandwiched by AC5 on both sides (Fig. 1e). The BT and AC2 domains of the two protomers form a platform, keeping the BC domain dimer in place and possibly also helping with BC domain dimerization (Fig. 1b). The conformational variability observed for the domains in the central region (Extended Data Fig. 9) might have a role in regulating the activity of the holoenzyme.

The structural analysis indicates that BCCP-biotin becomes carboxylated in the BC active site of its own protomer, and then translocates to the CT active site at the dimer interface, where it contacts the C domain of the other protomer (Fig. 4). The distance between the BC and CT active sites is  $\sim 80 \text{ \AA}$ , indicating that the entire BCCP domain must translocate during catalysis (swinging-domain model, Extended Data Fig. 4), as has been observed in the other holoenzymes<sup>1,9–14</sup>. In fact, the linker from BT to BCCP (residues 697–700) is about  $45 \text{ \AA}$  from the N1' atom of biotin, and therefore a rotation of this linker by  $\sim 180^\circ$  could bring the biotin into the BC active site from the CT active site (Fig. 4). The linker from BCCP to AC1 (residues 770–795) is much longer and can accommodate such a rotation, and part of this linker is disordered in the current structure.

We introduced mutations in the interfaces in the holoenzyme to assess the structural information. The mutants that could be purified migrated at the same position on a gel filtration column and had nearly the same thermal melting curves as the wild-type enzyme (data not shown). Deletion of the  $\alpha$ -helical hairpin ( $\alpha 8$ – $\alpha 9$ , residues 940–972) in domain AC1 (Extended Data Fig. 2) or the  $\beta 4A$ – $\beta 4B$  loop in the C domain of CT (residues 1902–1916, Extended Data Fig. 3) abolished the catalytic activity (Table 1), demonstrating their importance in anchoring the hook of the BT domain (Fig. 2b). On the other hand, mutating Gln608 in the hook, which interacts with the main chain of

**Table 1 | Effects of mutations in the ScACC holoenzyme interfaces on the catalysis**

Enzyme	$K_m$ (mM)*	$k_{cat}$ (s <sup>-1</sup> )
Wild-type ScACC	$0.053 \pm 0.011$	$8.5 \pm 0.4$
$\Delta 940$ – $972$ ( $\alpha 8$ – $\alpha 9$ hairpin of AC1)	No activity detected	
$\Delta 1902$ – $1916$ ( $\beta 4A$ – $\beta 4B$ loop of CT)	No activity detected	
$\Delta 836$ – $918$ (AC2)	No expression	
K73E	Very low activity	
R76E	No activity detected	
Y83A	$0.074 \pm 0.020$	$1.6 \pm 0.1$
W487A	Very low activity	
Q608R	$0.11 \pm 0.02$	$16 \pm 1.0$
R656E	$0.15 \pm 0.07$	$5.0 \pm 0.6$

\*The errors were obtained from fitting data to the Michaelis–Menten equation.

the  $\beta$ 4A– $\beta$ 4B loop (Fig. 2b), had little effect on catalysis. Similarly, the R656E mutation at the edge of the BT–BC interface (Fig. 2a) had little effect, suggesting that these single-site mutations are not sufficient to disrupt the holoenzyme or that these regions of contact do not contribute significantly to the interactions.

We introduced the K73E, R76E and W487A mutations in the BC domain dimer interface (Extended Data Fig. 7), and all three essentially abolished the catalytic activity (Table 1). The mutations probably disrupted the BC domain dimer, and the domain changed to the other conformation that is incompatible with catalysis. The K73E and R76E mutants are equivalent to the R16E and R19E mutants of *E. coli* BC subunit that we characterized earlier<sup>25,29</sup>. Those mutations greatly destabilized the dimer, but had only a small effect (about three-fold) on the catalytic activity of the BC subunit alone, probably because the *E. coli* BC monomer does not undergo the conformational transition as observed here for the eukaryotic BC (Fig. 3e). However, the R19E mutation had a much larger effect *in vivo*, probably in the context of the *E. coli* ACC holoenzyme<sup>30</sup>.

Overall, our studies have produced the first structural information on the 500-kDa yeast ACC holoenzyme dimer. This structure is likely to have relevance for other eukaryotic ACCs, especially the human ACC holoenzymes, as they share 45% sequence identity with yeast ACC. The structures of the BC and CT domains of human and yeast ACCs are highly similar and consistent with their strong sequence conservation (Extended Data Figs 1, 3). Although the sequence conservation for the central region is weaker, the secondary structure elements in yeast ACC are predicted to be present in human ACC as well, and residues in these secondary structure elements are more conserved than those in the loops (Extended Data Fig. 2). Therefore, the overall structure of human ACC holoenzyme is likely to be similar to that of yeast ACC.

**Online Content** Methods, along with any additional Extended Data display items and Source Data, are available in the online version of the paper; references unique to these sections appear only in the online paper.

Received 22 March; accepted 4 August 2015.

Published online 12 October 2015.

- Tong, L. Structure and function of biotin-dependent carboxylases. *Cell. Mol. Life Sci.* **70**, 863–891 (2013).
- Waldrop, G. L., Holden, H. M. & St Maurice, M. The enzymes of biotin dependent CO<sub>2</sub> metabolism: what structures reveal about their reaction mechanisms. *Protein Sci.* **21**, 1597–1619 (2012).
- Cronan, J. E. Jr & Waldrop, G. L. Multi-subunit acetyl-CoA carboxylases. *Prog. Lipid Res.* **41**, 407–435 (2002).
- Polyak, S. W., Abell, A. D., Wilce, M. C. J., Zhang, L. & Booker, G. W. Structure, function and selective inhibition of bacterial acetyl-CoA carboxylase. *Appl. Microbiol. Biotechnol.* **93**, 983–992 (2012).
- Abramson, H. N. The lipogenesis pathway as a cancer target. *J. Med. Chem.* **54**, 5615–5638 (2011).
- Wakil, S. J. & Abu-Elheiga, L. A. Fatty acid metabolism: target for metabolic syndrome. *J. Lipid Res.* **50** (Suppl.), S138–S143 (2009).
- Schneiter, R. et al. A yeast acetyl coenzyme A carboxylase mutant links very-long-chain fatty acid synthesis to the structure and function of the nuclear membrane-pore complex. *Mol. Cell. Biol.* **16**, 7161–7172 (1996).
- Hoja, U., Wellein, C., Greiner, E. & Schweizer, E. Pleiotropic phenotype of acetyl-CoA-carboxylase-defective yeast cells. *Eur. J. Biochem.* **254**, 520–526 (1998).
- St Maurice, M. et al. Domain architecture of pyruvate carboxylase, a biotin-dependent multifunctional enzyme. *Science* **317**, 1076–1079 (2007).
- Xiang, S. & Tong, L. Crystal structures of human and *Staphylococcus aureus* pyruvate carboxylase and molecular insights into the carboxyltransfer reaction. *Nature Struct. Mol. Biol.* **15**, 295–302 (2008).
- Huang, C. S. et al. Crystal structure of the  $\alpha_6\beta_6$  holoenzyme of propionyl-coenzyme A carboxylase. *Nature* **466**, 1001–1005 (2010).
- Huang, C. S., Ge, P., Zhou, Z. H. & Tong, L. An unanticipated architecture of the 750-kDa  $\alpha_6\beta_6$  holoenzyme of 3-methylcrotonyl-CoA carboxylase. *Nature* **481**, 219–223 (2012).

- Fan, C., Chou, C.-Y., Tong, L. & Xiang, S. Crystal structure of urea carboxylase provides insights into the carboxyltransfer reaction. *J. Biol. Chem.* **287**, 9389–9398 (2012).
- Tran, T. H. et al. Structure and function of a single-chain, multi-domain long-chain acyl-CoA carboxylase. *Nature* **518**, 120–124 (2015).
- Weatherly, S. C., Volrath, S. L. & Elich, T. D. Expression and characterization of recombinant fungal acetyl-CoA carboxylase and isolation of a soraphen-binding domain. *Biochem. J.* **380**, 105–110 (2004).
- Shen, Y., Volrath, S. L., Weatherly, S. C., Elich, T. D. & Tong, L. A mechanism for the potent inhibition of eukaryotic acetyl-coenzyme A carboxylase by soraphen A, a macrocyclic polyketide natural product. *Mol. Cell* **16**, 881–891 (2004).
- Zhang, H., Yang, Z., Shen, Y. & Tong, L. Crystal structure of the carboxyltransferase domain of acetyl-coenzyme A carboxylase. *Science* **299**, 2064–2067 (2003).
- Chapman-Smith, A., Forbes, B. E., Wallace, J. C. & Cronan, J. E. Jr. Covalent modification of an exposed surface turn alters the global conformation of the biotin carrier domain of *Escherichia coli* acetyl-CoA carboxylase. *J. Biol. Chem.* **272**, 26017–26022 (1997).
- Solbiati, J., Chapman-Smith, A. & Cronan, J. E. Jr. Stabilization of the biotinoyl domain of *Escherichia coli* acetyl-CoA carboxylase by interactions between the attached biotin and the protruding “thumb” structure. *J. Biol. Chem.* **277**, 21604–21609 (2002).
- Hung, C. L. et al. Crystal structure of *Helicobacter pylori* formamidase AmiF reveals a cysteine–glutamate–lysine catalytic triad. *J. Biol. Chem.* **282**, 12220–12229 (2007).
- Holm, L., Kääriäinen, S., Rosenström, P. & Schenkel, A. Searching protein structure databases with DALI-Lite v3. *Bioinformatics* **24**, 2780–2781 (2008).
- Raymer, B. et al. Synthesis and characterization of a BODIPY-labeled derivative of Soraphen A that binds to acetyl-CoA carboxylase. *Bioorg. Med. Chem. Lett.* **19**, 2804–2807 (2009).
- Cho, Y. S. et al. Molecular mechanism for the regulation of human ACC2 through phosphorylation by AMPK. *Biochem. Biophys. Res. Commun.* **391**, 187–192 (2010).
- Waldrop, G. L., Rayment, I. & Holden, H. M. Three-dimensional structure of the biotin carboxylase subunit of acetyl-CoA carboxylase. *Biochemistry* **33**, 10249–10256 (1994).
- Shen, Y., Chou, C.-Y., Chang, G.-G. & Tong, L. Is dimerization required for the catalytic activity of bacterial biotin carboxylase? *Mol. Cell* **22**, 807–818 (2006).
- Chou, C.-Y., Yu, L. P. C. & Tong, L. Crystal structure of biotin carboxylase in complex with substrates and implications for its catalytic mechanism. *J. Biol. Chem.* **284**, 11690–11697 (2009).
- Harwood, H. J. Jr et al. Isozyme-nonselective N-substituted bipiperidylcarboxamide acetyl-CoA carboxylase inhibitors reduce tissue malonyl-CoA concentrations, inhibit fatty acid synthesis, and increase fatty acid oxidation in cultured cells and in experimental animals. *J. Biol. Chem.* **278**, 37099–37111 (2003).
- Zhang, H., Tweel, B., Li, J. & Tong, L. Crystal structure of the carboxyltransferase domain of acetyl-coenzyme A carboxylase in complex with CP-640186. *Structure* **12**, 1683–1691 (2004).
- Chou, C.-Y. & Tong, L. Structural and biochemical studies on the regulation of biotin carboxylase by substrate inhibition and dimerization. *J. Biol. Chem.* **286**, 24417–24425 (2011).
- Smith, A. C. & Cronan, J. E. Dimerization of the bacterial biotin carboxylase subunit is required for acetyl coenzyme A carboxylase activity *in vivo*. *J. Bacteriol.* **194**, 72–78 (2012).

**Supplementary Information** is available in the online version of the paper.

**Acknowledgements** We thank M. Bush, C.-Y. Chou, Y. Shen, L. Yu and H. Zhang for carrying out initial studies in this project; R. Jackimowicz, B. Nolan, N. Whalen, A. Heroux and H. Robinson for access to the X29A and X25 beamlines at the NSLS; S. Banerjee, K. Perry, R. Rajashankar, J. Schuermann, N. Sukumar for access to NE-CAT 24-C and 24-E beamlines at the Advanced Photon Source; W. Rice and E. Eng at New York Structural Biology Center for assistance with electron microscopy. The in-house X-ray diffraction instrument was purchased with an NIH grant to L.T. (S100D012018). This research was supported in part by a grant from the NIH (R01DK067238) to L.T.

**Author Contributions** J.W. carried out protein expression, purification, crystallization, data collection, structure determination and refinement, site-directed mutagenesis and enzymatic assays. L.T. initiated the project, supervised the entire research, and analysed the results. J.W. and L.T. wrote the paper.

**Author Information** Coordinates and structure factors have been deposited in the Protein Data Bank under accession numbers 5CS0 for AC1–AC2, 5CS4 for AC3–AC5, 5CSA for BT–BCCP–AC1–AC5, 5CSK for unbiotinylated ACC, and 5CSL for ACC holoenzyme. Reprints and permissions information is available at [www.nature.com/reprints](http://www.nature.com/reprints). The authors declare no competing financial interests. Readers are welcome to comment on the online version of the paper. Correspondence and requests for materials should be addressed to L.T. (ltong@columbia.edu).

## METHODS

**Protein expression and purification.** The N-terminal segment of the central region of *Saccharomyces cerevisiae* ACC (ScACC, gene *ACC1*, residues 797–1033, AC1–AC2 domains) was expressed at 20 °C in *E. coli* BL21(DE3) Star cells for native protein or B384(DE3) cells for selenomethionyl protein, in the presence of a chaperone plasmid pG-KJE8 (TaKaRa). The recombinant protein carried a C-terminal His-tag and was purified by Ni-NTA (Qiagen) and gel filtration chromatography (Sephacryl S-300, GE Healthcare) in buffer A (20 mM Tris (pH 7.5), 300 mM NaCl, and 2 mM DTT).

The C-terminal segment of the central region of ScACC (residues 1036–1503, AC3–AC5 domains) was expressed in *E. coli* B834(DE3) cells at 25 °C for selenomethionyl protein and purified following the same protocol. The gel filtration buffer contained 10 mM rather than 2 mM DTT.

The segment containing the BT–BCCP–AC1–AC5 domains of ScACC (residues 569–1494) was expressed in BL21(DE3) Rosetta cells at 24 °C. The recombinant protein, with a C-terminal His-tag, was purified by Ni-NTA and gel filtration chromatography in buffer A.

Full-length ScACC (residues 1–2233) was constructed into pET28a (Novagen) by sewing together two PCR fragments with a 900-nt overlap. For structure determination, the segment containing residues 22–2233, with a C-terminal His-tag, was expressed in *E. coli* BL21(DE3) Star cells at 25 °C. Protein expression for all the different ScACC segments was driven by the *trp* promoter and was induced with 3-indoleacrylic acid. However, the endogenous *E. coli* biotin-protein ligase (BPL, also known as BirA) was not able to biotinylate the ScACC. The ScBPL gene was amplified from the genome and inserted into the pCDFDuet-1 vector (Novagen) multiple cloning site 2 without any affinity tag. Co-expression of ScBPL and the inclusion of 20 mg l<sup>-1</sup> biotin in the media allowed complete biotinylation of ScACC, confirmed by an avidin shift assay. The protein was purified by Ni-NTA and gel filtration chromatography in buffer A. Typically 0.5 mg of biotinylated ScACC (or 3 mg of unbiotinylated ScACC) could be purified from 12 l of culture.

**Protein crystallization.** Crystals were obtained at 20 °C using the sitting-drop vapour diffusion method. Native and selenomethionyl crystals of the AC1–AC2 domains were obtained using a precipitant solution of 90 mM Bis-tris propane and 60 mM citric acid (pH 6.4), and 20% (w/v) PEG3350. The protein concentration was 12 mg ml<sup>-1</sup>, and the crystals took 3 weeks to reach full size.

Selenomethionine-substituted crystals of the AC3–AC5 domains were obtained after 2 days. The protein concentration was 3.6 mg ml<sup>-1</sup>, and the precipitant solution contained 80 mM HEPES (pH 7.5), 4% (v/v) MPD, 8 mM sodium citrate, 4% (v/v) glycerol, and 40 mM NDSB-201.

Native crystals of the BT–BCCP–AC1–AC5 domains were obtained after 4 days. The protein concentration was 15 mg ml<sup>-1</sup>, and the precipitant solution contained 80 mM HEPES (pH 7.5), 9.6% (w/v) PEG6000, 1.6% (v/v) MPD, 60 mM sodium citrate, and 80 mM NaI.

Full-length ACC protein was incubated with 3.3 mM acetyl-CoA and 3.3 mM Mg-ADP for 30 min on ice before crystallization. Crystals were obtained after 2 weeks. The protein concentration was 5 mg ml<sup>-1</sup>, and the precipitant solution contained 14% (w/v) PEG3350, 4% (v/v) tert-butanol, and 0.2 M sodium citrate.

Glycerol was used as the cryo-protectant and all crystals were flash frozen in liquid nitrogen for data collection at 100 K.

**Data collection and structure determination.** X-ray diffraction data of AC1–AC2 domains were collected on an ADSC Q315 CCD at the X29A beamline of the National Synchrotron Light Source (NSLS). The diffraction images were processed with the HKL program<sup>31</sup>. The crystal belonged to space group *P*6<sub>5</sub> with cell parameters of *a* = *b* = 117.6 Å, and *c* = 73.8 Å. There is a domain-swapped dimer of the protein in the asymmetric unit. A selenomethionyl single-wavelength anomalous diffraction (SAD) data set was collected to 3.0 Å resolution (wavelength 0.979 Å) and a native data set to 2.5 Å resolution (wavelength 1.075 Å). Five Se atoms were located with program Solve<sup>32</sup> and used for phasing with program Phenix<sup>33</sup>. The phase information was then extended to 2.5 Å with solvent flattening, histogram matching and two-fold non-crystallographic symmetry (NCS) averaging using the program DM in CCP4<sup>34</sup>. The atomic model was built into the electron density map manually with the program Coot<sup>35</sup>. Structure refinement was performed with CNS<sup>36</sup> and Refmac5<sup>37</sup>.

A selenomethionyl SAD data set to 3.2 Å resolution of AC3–AC5 domains was collected at the X29A beamline (wavelength 0.979 Å). The crystal belonged to space group *P*2<sub>1</sub>, with cell parameters of *a* = 56.8 Å, *b* = 93.3 Å, *c* = 111.1 Å, and  $\beta$  = 100.6°. There are two molecules in the asymmetric unit. Five Se atoms in each molecule were located and employed for phasing with program Phenix. An atomic model was manually built into the electron density map with program Coot, and the structure was refined with Refmac5.

A native diffraction data set to 3.0 Å resolution of BT–BCCP–AC1–AC5 domains was collected at the X29A beamline (wavelength 1.075 Å). The crystal belonged to space group *P*2<sub>1</sub>, with cell parameters of *a* = 93.3 Å, *b* = 149.7 Å, *c* = 95.4 Å, and  $\beta$  = 118.4°. There is a dimer of the protein in the asymmetric unit. The structures of AC1–AC2 and AC3–AC5 domains were used as the search models to solve the structure by molecular replacement with the program Phaser<sup>38</sup>. The BT and BCCP domains were manually built into the electron density map.

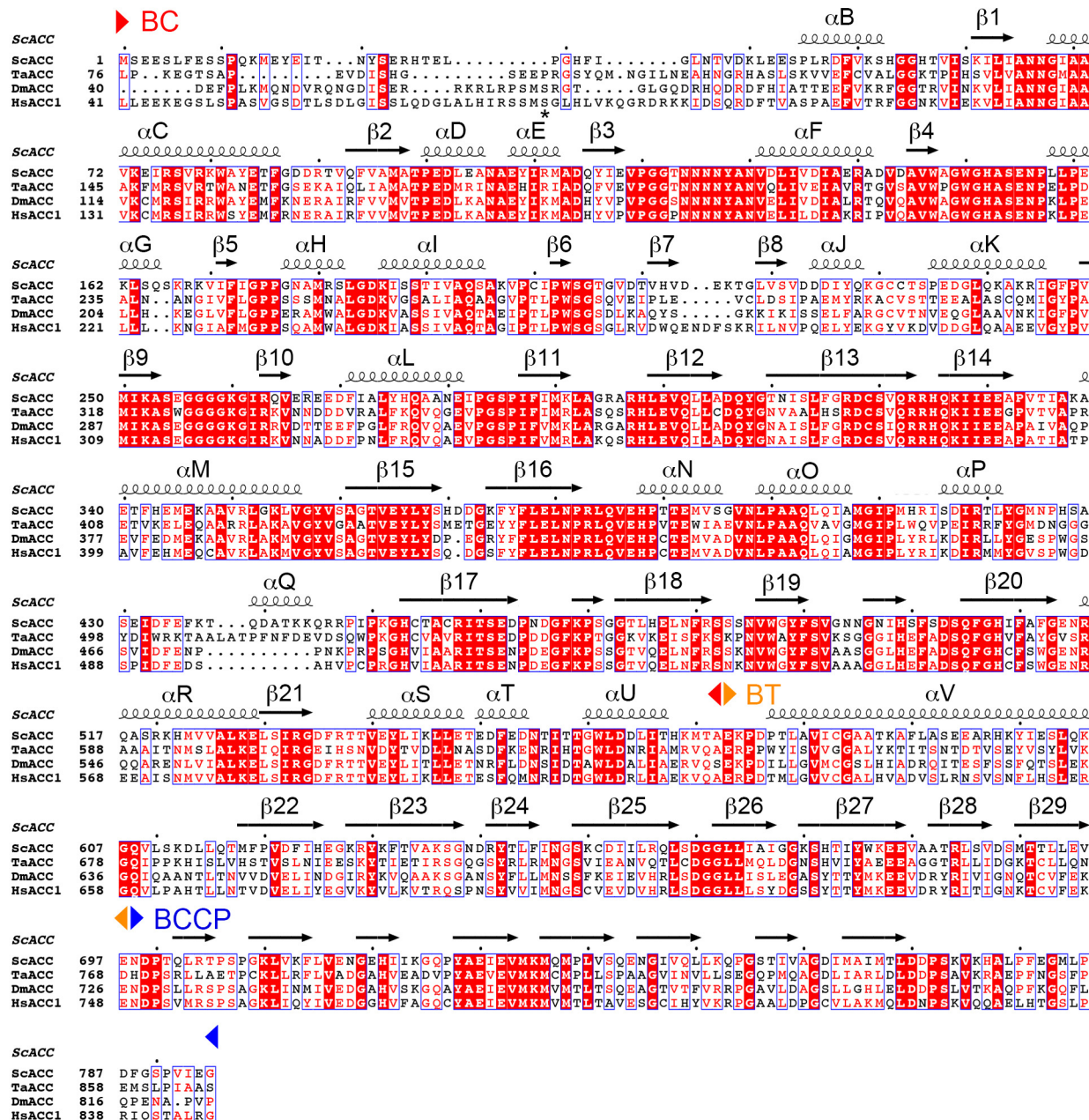
A native diffraction data set to 3.1 Å resolution of residues 22–2233 of unbiotinylated ScACC was collected on a Pilatus 6M detector at the X25 beamline of NSLS (wavelength 1.100 Å). There is a dimer of ScACC in the asymmetric unit. The structure was solved by molecular replacement with the program Phaser. The structures of AC1–AC2, AC3–AC5, and BT domains reported here and previously published structures of yeast BC<sup>16</sup> and CT domains<sup>17</sup> were used as the search models. However, no electron density for the BCCP domain was observed based on the crystallographic analysis.

A native diffraction data set to 3.2 Å resolution of biotinylated ScACC was collected at the X25 beamline. The crystal belonged to space group *P*4<sub>2</sub>2<sub>1</sub>, with cell parameters of *a* = *b* = 159.9 Å, and *c* = 614.4 Å, isomorphous to that of the unbiotinylated ScACC. The final atomic model was built with Coot and refined with Refmac5. NCS restraints were used during the refinement. Crystals of full-length ScACC (residues 1–2233) did not diffract beyond 8 Å resolution even after extensive efforts. The geometry of the final model was validated with MolProbity<sup>39</sup>.

**Mutagenesis and kinetic assays.** Site-specific and deletion mutations were introduced with the QuikChange kit (Agilent) and sequenced for confirmation. In deletion mutants, residues 940–972 of the  $\alpha$ -helical hairpin ( $\alpha$ 8– $\alpha$ 9) in domain AC1 and residues 836–918 in domain AC2 were replaced by a (GS)<sub>3</sub> linker, respectively, while residues 1902–1916 of the  $\beta$ 4A– $\beta$ 4B loop in the C domain of CT were replaced by a (GS)<sub>2</sub> linker.

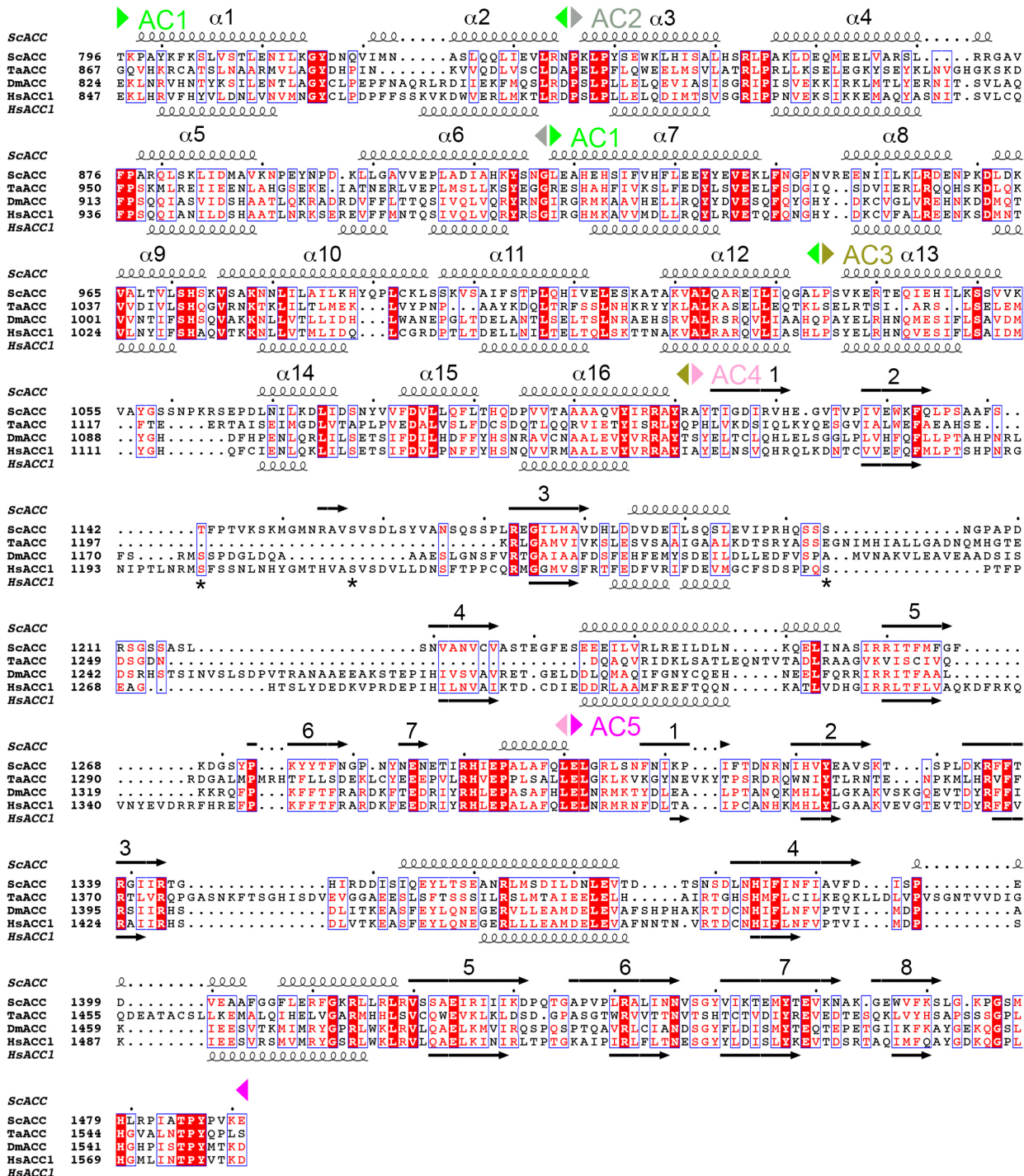
The catalytic activity of ACC was determined using a coupled enzyme assay, converting the hydrolysis of ATP to the disappearance of NADH<sup>40</sup>. The reaction mixture contained 100 mM HEPES (pH 7.5), 8 mM MgCl<sub>2</sub>, 40 mM KHCO<sub>3</sub>, 200 mM KCl, 0.2 mM NADH, 0.5 mM phosphoenolpyruvate, 0.5 mM ATP, 6 units of lactate dehydrogenase (Sigma), 4 units of pyruvate kinase, 100 nM ACC and various concentrations of acetyl-CoA. The absorbance at 340 nm was monitored for 60 s.

31. Otwinowski, Z. & Minor, W. Processing of X-ray diffraction data collected in oscillation mode. *Methods Enzymol.* **276**, 307–326 (1997).
32. Terwilliger, T. C. SOLVE and RESOLVE: automated structure solution and density modification. *Methods Enzymol.* **374**, 22–37 (2003).
33. Adams, P. D. et al. PHENIX: building new software for automated crystallographic structure determination. *Acta Crystallogr. D* **58**, 1948–1954 (2002).
34. Collaborative Computational Project, Number 4. The CCP4 suite: programs for protein crystallography. *Acta Crystallogr. D* **50**, 760–763 (1994).
35. Emsley, P. & Cowtan, K. Coot: model-building tools for molecular graphics. *Acta Crystallogr. D* **60**, 2126–2132 (2004).
36. Brünger, A. T. et al. Crystallography & NMR system: A new software suite for macromolecular structure determination. *Acta Crystallogr. D* **54**, 905–921 (1998).
37. Murshudov, G. N., Vagin, A. A. & Dodson, E. J. Refinement of macromolecular structures by the maximum-likelihood method. *Acta Crystallogr. D* **53**, 240–255 (1997).
38. McCoy, A. J. et al. Phaser crystallographic software. *J. Appl. Cryst.* **40**, 658–674 (2007).
39. Chen, V. B. et al. MolProbity: all-atom structure validation for macromolecular crystallography. *Acta Crystallogr. D* **66**, 12–21 (2010).
40. Blanchard, C. Z., Lee, Y. M., Frantom, P. A. & Waldrop, G. L. Mutations at four active site residues of biotin carboxylase abolish substrate-induced synergism by biotin. *Biochemistry* **38**, 3393–3400 (1999).
41. Gouet, P., Courcelle, E., Stuart, D. I. & Métoz, F. ESPript: analysis of multiple sequence alignments in PostScript. *Bioinformatics* **15**, 305–308 (1999).



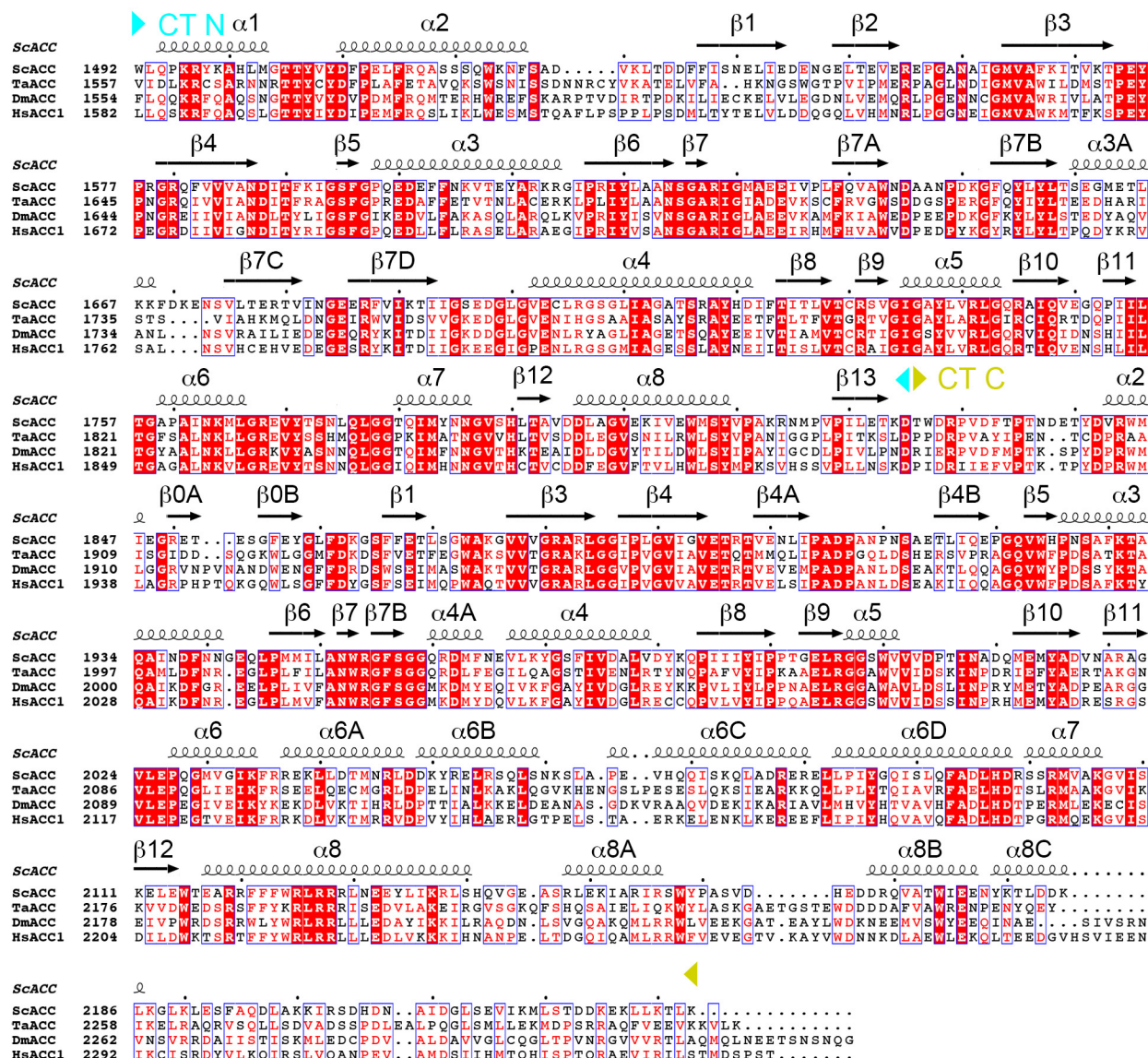
**Extended Data Figure 1 | Sequence alignment of the N-terminal region of eukaryotic, single-chain ACCs.** The region includes BC, BT and BCCP domains (indicated). The secondary structure elements in the ScACC holoenzyme structure are shown. The site of phosphorylation in HsACC1

(Ser80) is indicated with a star. This site does not exist in ScACC. ScACC, *Saccharomyces cerevisiae* ACC; TaACC, *Triticum aestivum* (wheat) ACC; DmACC, *Drosophila melanogaster* ACC; HsACC1, *Homo sapiens* ACC1. Modified from an output from ESPript<sup>41</sup>.

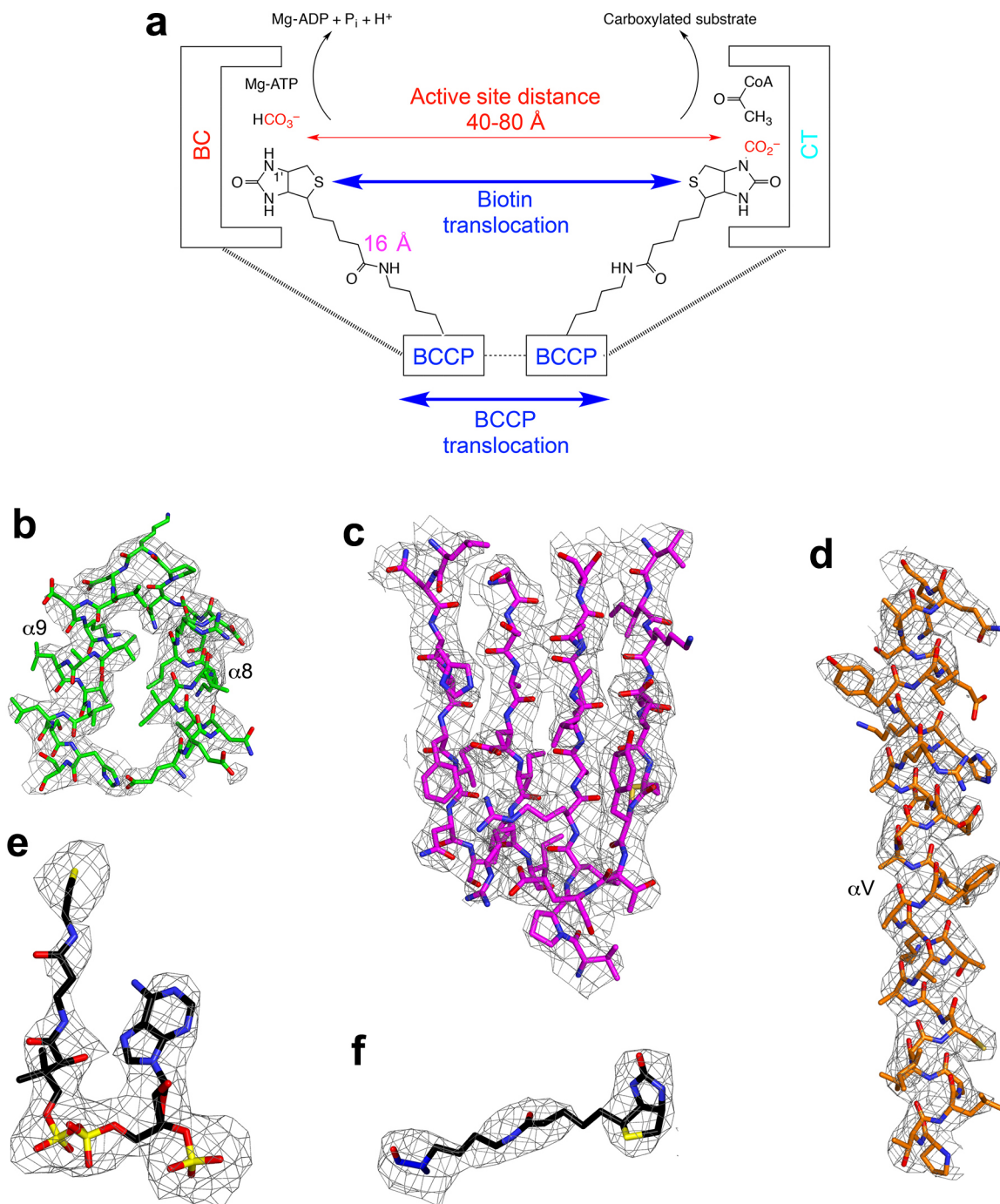


**Extended Data Figure 2 | Sequence alignment of the central region of eukaryotic, single-chain ACCs.** The AC1–AC5 domains are indicated. Predicted secondary structure elements in HsACC1 are also shown,

and they generally match those in the structure of ScACC. The helices in AC1–AC3 are numbered consecutively. Three sites of phosphorylation in HsACC1 are indicated with stars.

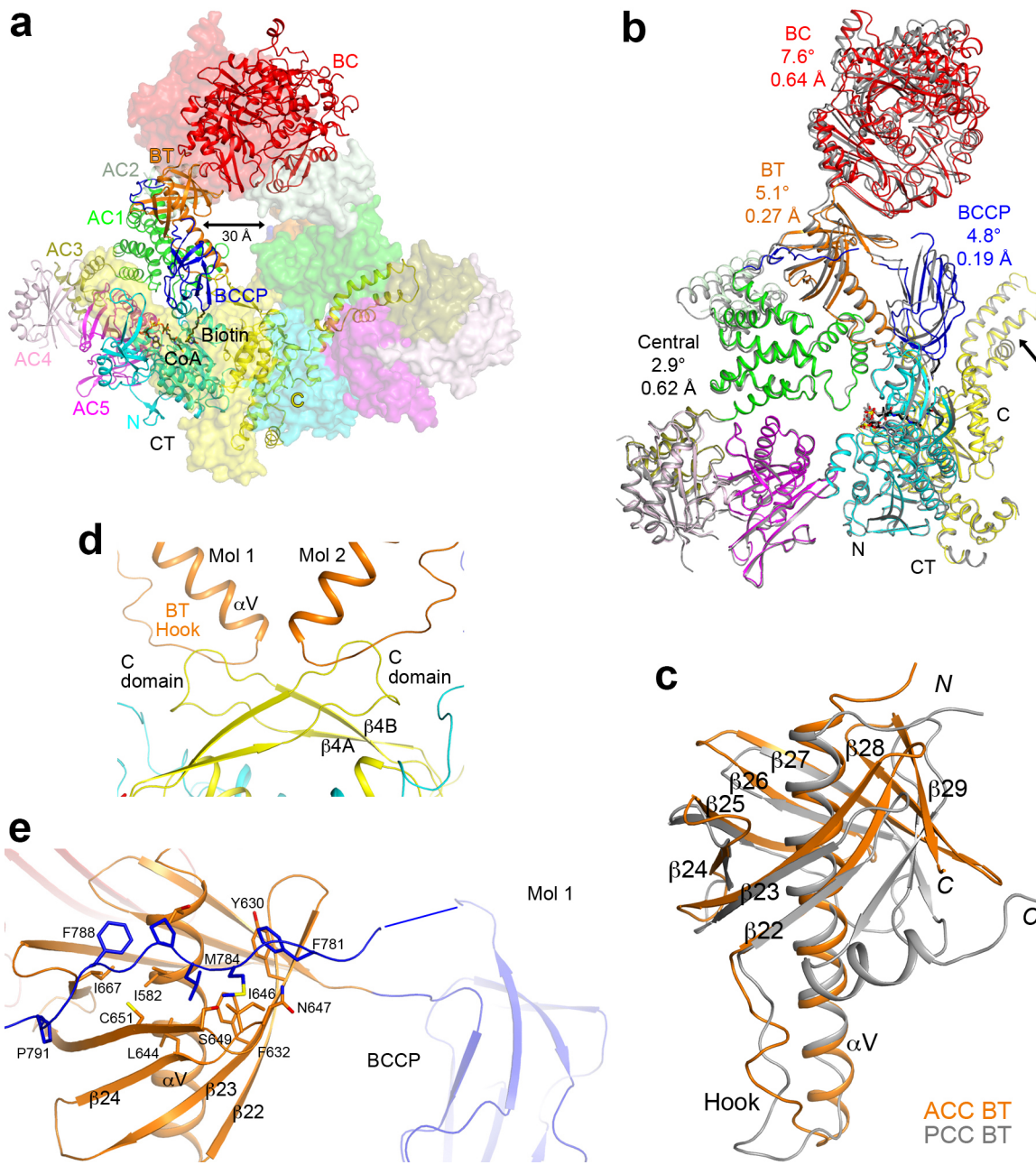


**Extended Data Figure 3 | Sequence alignment of the C-terminal region of eukaryotic, single-chain ACCs.** The region includes N and C domains of CTC (indicated).



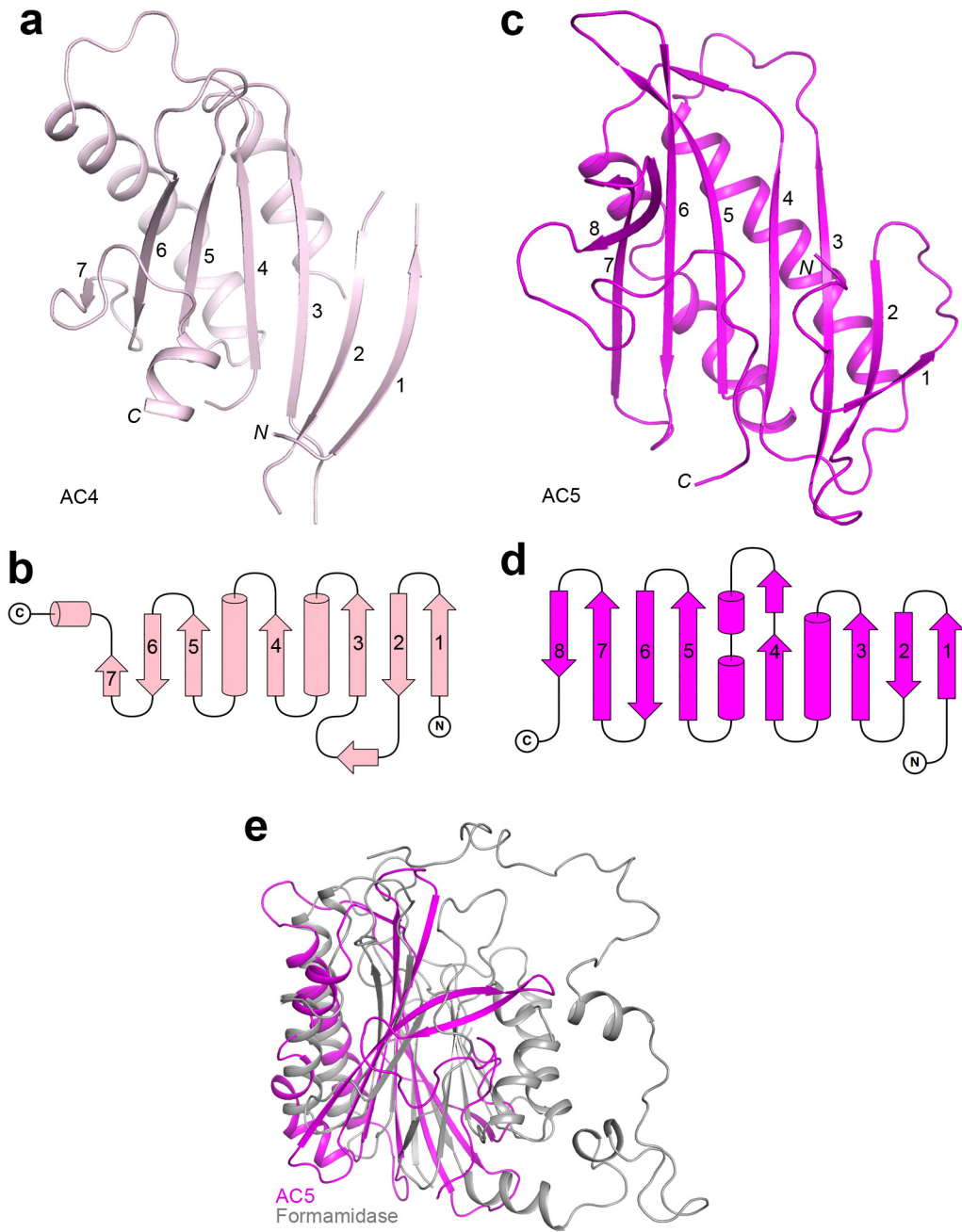
**Extended Data Figure 4 | Electron density for various regions of the ScACC holoenzyme structure.** **a**, Schematic of the two-step reaction in the catalysis by biotin-dependent carboxylases. Biotin is carboxylated in the BC active site, and then translocates to the CT active site where the substrate is carboxylated. The longest distance from the N1' atom of biotin to the C<sub>α</sub> atom of the Lys residue covalently attached to biotin is ~16 Å, giving a reach of ~30 Å for biotin (swinging-arm model). The actual distance between the BC

and CT active sites are larger than 30 Å, suggesting that BCCP needs to translocate in addition to the biotin (swinging-domain model). **b**,  $2F_o - F_c$  electron density for the helical hairpin insert ( $\alpha 8-\alpha 9$ ) of domain AC1 at 3.2 Å resolution, contoured at  $1\sigma$ . **c**,  $2F_o - F_c$  electron density for the  $\beta$ -sheet of domain AC5. **d**,  $2F_o - F_c$  electron density for the central helix ( $\alpha V$ ) of the BT domain. **e**, Omit  $F_o - F_c$  electron density for CoA at 3.2 Å resolution, contoured at  $2.5\sigma$ . **f**, Omit  $F_o - F_c$  electron density for biotin at 3.2 Å resolution.



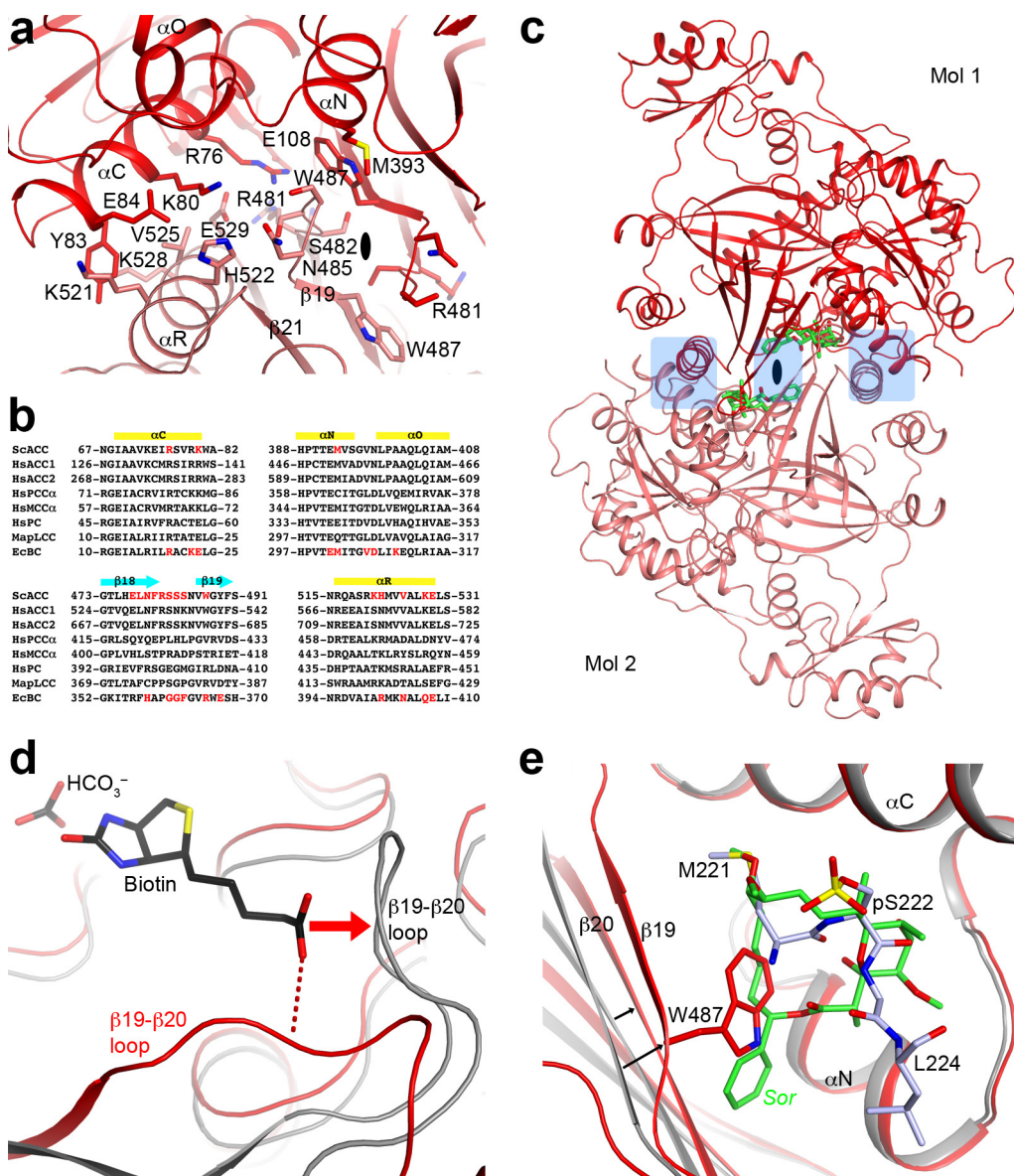
**Extended Data Figure 5 | Overall structure of the ScACC holoenzyme.** **a**, A large channel in the centre of the ScACC holoenzyme dimer. The view is related to that of Fig. 1b by an  $\sim 30^\circ$  rotation around the vertical axis. **b**, Overlay of the structures of the two protomers of ScACC holoenzyme dimer. One protomer is shown in colour and other in grey. The overlay is based on the CT domain. Differences in the orientations of the other domains are indicated, as well as the r.m.s. distance for their equivalent C $\alpha$  atoms. The arrow points to conformational differences in the insert domain of CT, linked to differences in the BCCP binding mode. **c**, Overlay of the BT domain of ScACC (in orange)

and the BT domain of PCC (in grey). The ‘hook’, connecting the end of the helix ( $\alpha$ V) to the first strand of the  $\beta$ -barrel ( $\beta$ 22), is labelled. The last three strands of the  $\beta$ -barrel ( $\beta$ 27– $\beta$ 29) are splayed further away from the central helix in ScACC compared to PCC. **d**, Interactions between the hook of the BT domain and the  $\beta$ 4A– $\beta$ 4B loop from the C domain of CT, an inserted segment that projects away from the rest of the domain. **e**, The BCCP-AC1 linker has hydrophobic interactions with the top of one side of the BT domain  $\beta$ -barrel. The disordered segment of the linker is indicated with the blue line.



**Extended Data Figure 6 | Domains AC4 and AC5 share a common backbone fold.** **a**, Structure of AC4 domain of ScACC. **b**, Topological drawing of AC4 domain. **c**, Structure of AC5 domain. **d**, Topological drawing of

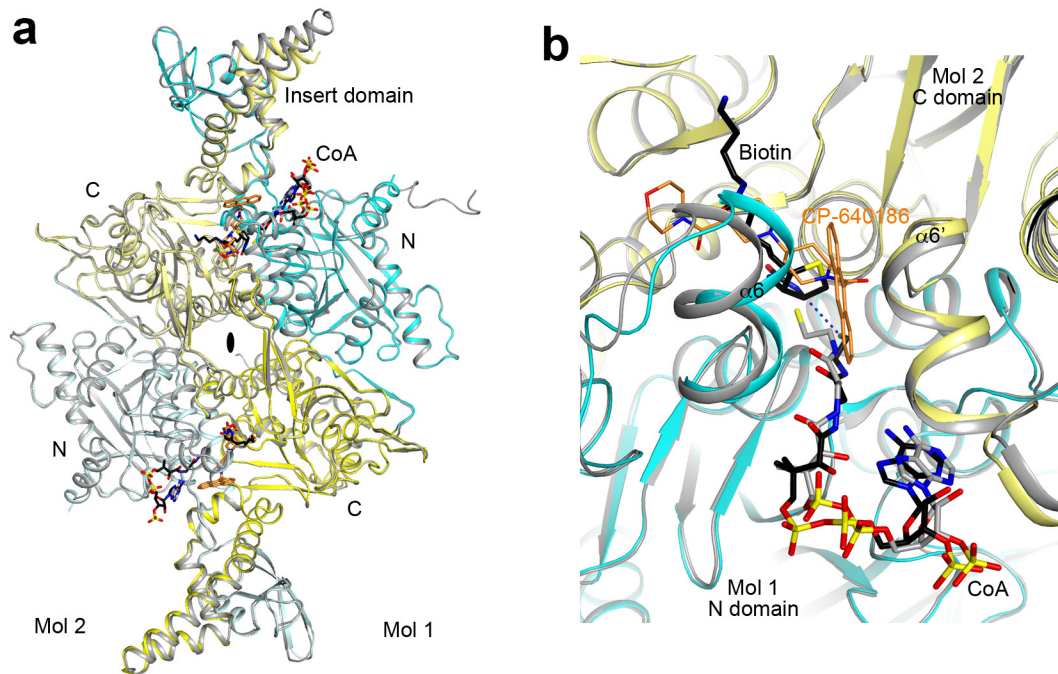
AC5 domain. **e**, Overlay of the structures of AC5 domain (magenta) and formamidase (grey). Formamidase has a four-layered  $\alpha\beta\beta\alpha$  structure, and AC5 matches only half of the structure.



**Extended Data Figure 7 | Structure of the BC domain dimer of ScACC.**

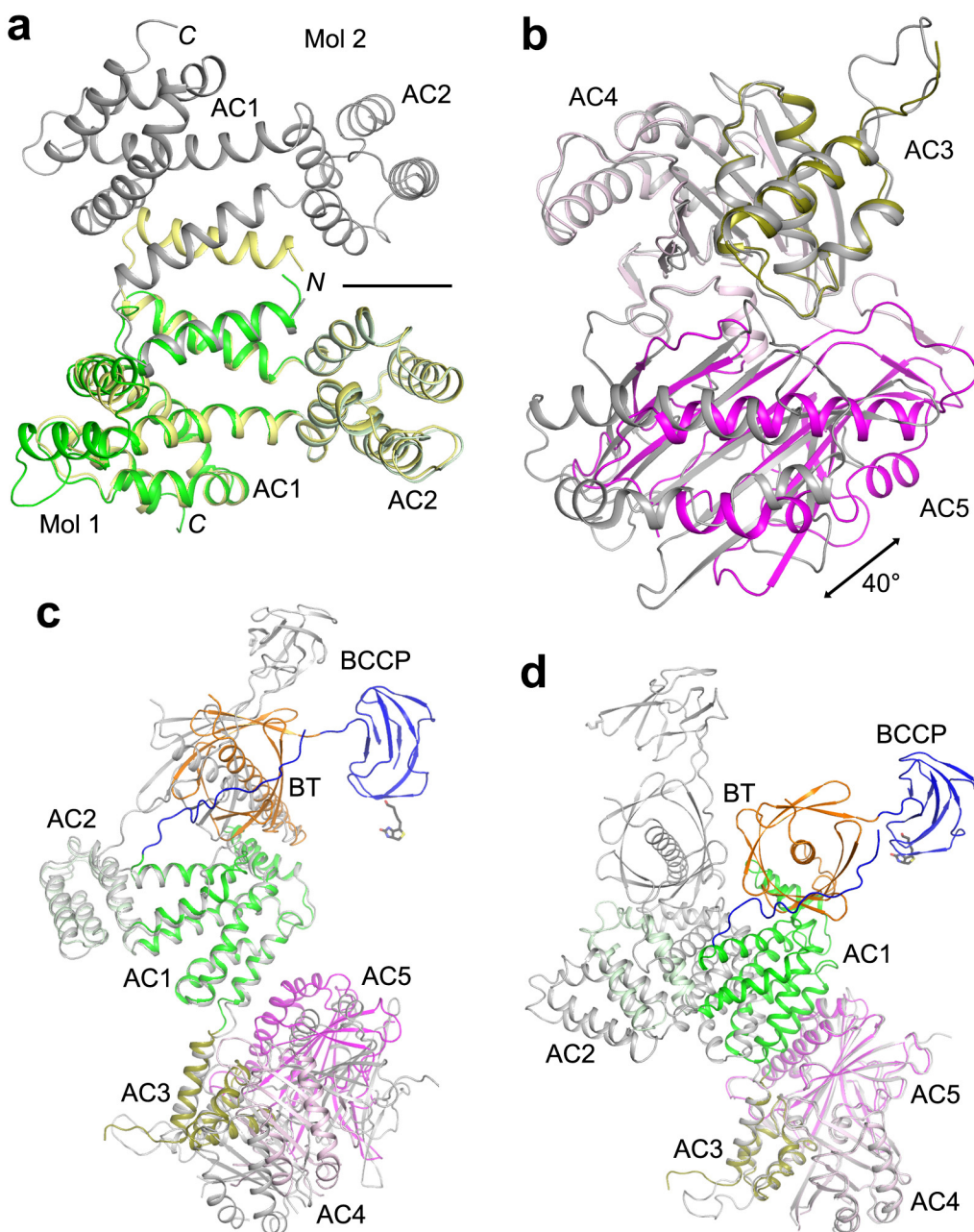
**a**, Interactions in the BC domain dimer interface. The BC domain of protomer 1 is in red, and that of protomer 2 in pink. **b**, Residues in the BC dimer interface (in red) of ScACC and *E. coli* BC (EcBC) are weakly conserved among the biotin-dependent carboxylases. MapLCC, long-chain acyl-CoA carboxylase of *Mycobacterium avium* subspecies *tuberculosis*. **c**, A BC domain dimer is constructed by superposing the structure of BC domain alone (in complex with soraphen A, green) onto that of the BC dimer. Regions of steric clashes between the two monomers are highlighted in light blue. **d**, Close-up view of the

binding site of biotin. The β19-β20 loop in the structure of BC domain alone (grey) clashes with biotin (red arrow), and cannot interact with the amide group of the biotin linkage (red dashed lines). **e**, Close-up view of the soraphen A (green) binding site. The movement of strands β19 and β20 from the structure of BC domain alone in complex with soraphen A (grey) is indicated with the arrows. Trp487 side chain in the holoenzyme structure clashes with soraphen A as well as the phosphorylated peptide segment containing pSer222 (light blue).



**Extended Data Figure 8 | Structure of the CT domain dimer of ScACC.**  
**a**, Overlay of the CT domain dimer in the ScACC holoenzyme (cyan and yellow for N and C domains of protomer 1, light cyan and light yellow for protomer 2) in complex with CoA (black) with the CT domain alone in complex with CoA (grey). Biotin is shown in black and BCCP is omitted for clarity. The bound position of the CP-640186 inhibitor (gold) is shown for reference. A conformational change for the insert domain at the top is due to the binding of BCCP in the holoenzyme, while the insert domain at the bottom shows

essentially no change because the BCCP–biotin is not bound as deeply into this active site. **b**, Overlay of the CT active site (cyan and yellow) of ScACC holoenzyme with that of CT alone in complex with CoA (grey). The CP-640186 inhibitor (gold) clashes with the bound position of biotin (black). The thiol group of CoA in the holoenzyme complex is 4.3 Å from the N<sub>1</sub> atom of biotin (dashed line in blue). The thiol group of CoA in the CT domain alone complex is in a different position, likely due to the absence of biotin in the active site.



**Extended Data Figure 9 | Comparisons of the structures of ACC central region alone with that in the holoenzyme.** **a**, Overlay of AC1–AC2 in the holoenzyme (colour) with AC1–AC2 alone (yellow and grey). The first helix is swapped between two monomers in the structure of AC1–AC2 alone, and the two-fold axis of that dimer is indicated with the black line. **b**, Overlay of AC3–AC5 in the holoenzyme (colour) with AC3–AC5 alone (grey), based on AC3–AC4. A large difference is seen for the orientation of AC5. **c**, Overlay of

BT–BCCP–AC1–AC5 in the holoenzyme (colour) with these domains alone (grey), based on AC1–AC2. Large differences are seen for BT, BCCP and AC3–AC5. **d**, Overlay of BT–BCCP–AC1–AC5 in the holoenzyme (colour) with these domains alone (grey), based on AC3–AC4. Large differences are seen for BT, BCCP and AC1–AC2, although AC5 has essentially the same position.

Extended Data Table 1 | Data collection and refinement statistics

	ScACC holoenzyme	ScACC (unbiotinylated)	AC1–AC2	AC3–AC5	BT–BCCP–AC1– AC5
<b>Data collection</b>					
Space group	<i>P</i> 4 <sub>3</sub> 2 <sub>1</sub> 2	<i>P</i> 4 <sub>3</sub> 2 <sub>1</sub> 2	<i>P</i> 6 <sub>5</sub>	<i>P</i> 2 <sub>1</sub>	<i>P</i> 2 <sub>1</sub>
Cell dimensions					
<i>a, b, c</i> (Å)	159.9, 159.9, 614.4	159.9, 159.9, 615.5	117.6, 117.6, 73.8	56.8, 93.3, 111.1	93.3, 149.7, 95.4
$\alpha, \beta, \gamma$ (°)	90, 90, 90	90, 90, 90	90, 90, 120	90, 100.6, 90	90, 118.4, 90
Resolution (Å)	50-3.2 (3.3-3.2)*	50-3.1 (3.2-3.1)	50-2.5 (2.6-2.5)	50-3.2 (3.3-3.2)	50-3.0 (3.1-3.0)
<i>R</i> <sub>merge</sub>	14.8 (90.1)	10.9 (88.1)	7.1 (41.6)	7.5 (40.5)	8.8 (44.9)
CC <sub>1/2</sub>	(0.448)	(0.452)		(0.965)	(0.848)
<i>I</i> / $\sigma$ <i>I</i>	7.0 (1.0)	8.2 (1.1)	18.6 (2.6)	21.9 (5.1)	13.7 (2.9)
Completeness (%)	98 (87)	93 (90)	100 (99)	100 (100)	99 (100)
Redundancy	3.0 (2.7)	2.3 (2.3)	4.2 (3.6)	7.6 (7.6)	3.4 (3.4)
<b>Refinement</b>					
Resolution (Å)	50-3.2	50-3.1	50-2.5	50-3.2	50-3.0
No. reflections	122,246	129,166	19,205	18,134	42,803
<i>R</i> <sub>work</sub> / <i>R</i> <sub>free</sub>	21.9 / 26.6	21.7 / 28.1	21.2 / 27.1	23.4 / 28.7	23.0 / 28.9
No. atoms					
Protein	32,651	31,816	3,370	6,353	13,699
Ligand/ion	126	0	0	0	0
Water	0	0	45	0	0
B-factors					
Protein	96.8	93.2	79.2	87.9	74.9
Ligand/ion	106.2	—	—	—	—
Water	—	—	61.0	—	—
R.m.s deviations					
Bond lengths (Å)	0.011	0.011	0.012	0.010	0.010
Bond angles (°)	1.5	1.5	1.4	1.4	1.3

One crystal was used for data collection.

\*Highest resolution shell is shown in parentheses.